

Observation of Quantum Coulomb Blockade Facilitated by P-Donor Molecules in Silicon Nano-Transistor

Soumya Chakraborty,^{*1}Pooja Sudha,^{*1}Hemant Arora,¹Daniel Moraru,² and Arup Samanta^{1,3,a)}

¹Quantum / Nano-science and Technology Lab, Department of Physics, Indian Institute of Technology Roorkee, Roorkee 247667, Uttarakhand, India

²Research Institute of Electronics, Shizuoka University, 3-5-1 Johoku, Chuo-ku, Hamamatsu 432-8011, Japan

³Centre of Nanotechnology, Indian Institute of Technology Roorkee, Roorkee 247667, Uttarakhand, India

^{a)}arup.samanta@ph.iitr.ac.in

Multi-donor architecture developed on the base of silicon technology holds significant potential towards room-temperature qubit and other single-electron tunneling (SET) functionalities. However, within such architecture, the overlap of multiple donor wave-functions results in a complex internal electronic configuration with discrete energy levels. Probing these discrete states, observed as multiple conductance peaks, is essential for understanding inter-donor coupling and exchange interactions towards coherent electron transfer. In this direction, we have experimentally demonstrated one-by-one electron filling within multiple-donor molecules with the fundamental analysis of clear and sustained quantum Coulomb blockade (QCB) effect. Moreover, the underlying physics of molecular orbitals, where the increasing energy leads to a larger spatial extent of the corresponding orbital, has been reflected by the systematic decrement of the respective charging-energies. The molecular energy levels, resulting from the orbital hybridization of individual donors, are also confirmed through first-principles simulations using density functional theory (DFT). Furthermore, Monte Carlo simulations based on the orthodox theory of Coulomb blockade support the observed QCB characteristics.

Quantum technologies, including quantum computers and advanced quantum-electronic devices, fundamentally rely on precise control of single electrons within quantum-confined systems. Scalable donor-based silicon (Si) architectures¹⁻⁶ are the cutting-edge advanced technology due to their atomic precision, enhanced stability, and compatibility with existing semiconductor technologies.⁷ Seamless operation of such sophisticated devices at elevated temperatures, against thermal fluctuations, requires sustained single-electron effects, but most reports are limited to temperatures of a few tens of Kelvin.⁸⁻¹¹ Although the leverage of confinement effects^{12,13} have facilitated high charging-energy (E_{ch}) and enhanced barrier heights to harness the high-temperature single-electron tunneling exploiting even via isolated donors,^{14,15} effectiveness and reproducibility of this approach is heavily impaired by the inherent challenges of nano-fabrication and precise dopant placement. A more effective strategy is to create a deep-level quantum dot (QD) by coupling a few closely-spaced donor-atoms, where the ground-state is found at energy far lower than the isolated-donor systems, resulting in enhanced electron charging energy and ionization energy (E_i), necessary for sustained Coulomb blockade (CB) at higher temperatures.¹⁶

However, in the closely-spaced multiple-donor molecule, donor's wave functions will superimpose to each other and resulting the splitting of individual-donor energy levels to a many-fold quantized energy spectrum. The ability to probe such discrete electronic states, often resolved as multiple conductance peaks in the transport characteristics of such devices, is critical for understanding the complex interplay between confinement potential and inter-donor coupling.¹⁷ Moreover, understanding the systematic one-by-one electron transport and filling within such a system with evolving external bias voltages are essential for coherent single-electron manipulation towards qubit operations. Although spin-blockade and quantum transport through multi-donor molecule have been reported,^{16,18} systematic investigation of electron filling and effect of each molecular energy levels on the charging and ionization energies is highly essential to develop the controlled quantum devices, as reported for the shell filling of electrons in a GaAs QD system.¹⁹

Here, we demonstrate the systematic one-by-one molecular filling of six electrons in the lowest-lying hybridized energy levels of each of the three isolated P-donor molecules formed within a Si nano-channel field-effect transistor. Moreover, the observed Quantum Coulomb Blockade (QCB) synchronizes precisely with the systematic evolution of available discrete excited states and the respective separation of energy levels (ΔE) that actively influences the transport characteristics, which had not been experimentally probed yet. Moreover, the

observed systematic decrement of E_{ch} , corresponding to higher energy levels with increasing Bohr radius (r_B) within the molecule, is well explained by the existing literature. The presented systematic study of the origin and dynamics of such donor-molecule states is expected to enhance the understanding of such complex systems towards their implementation in coherent single-electron technologies, even at elevated temperatures.

Donor potential distribution within a thin Si nano-channel

In this regard, we demonstrate single-electron transport in a nano-scale field-effect transistor (nano-FET) with lithographically-defined channel (~ 180 nm length, ~ 15 nm width, ~ 5 nm thickness), depicted schematically in Fig. 1a. A precisely defined 30 nm \times 15 nm region, 90 nm from the source, is selectively doped with phosphorus (P) donor concentration $N_D \approx 10^{19}$ cm⁻³, resulting in an average of ~ 22 randomly distributed donors (Figs. 1b-c). The corresponding inter-donor spacing of ~ 1.5 nm, significantly smaller than twice the Bohr radius, ~ 5 nm for isolated P-donors in bulk Si, would favor strong donor-donor coupling, enhancing cluster formation and artificial molecular states.²⁰

An instance of donor distribution and donor-induced potential landscape, exclusive of confinement effects, of the slit region are simulated within Figs. 1b-c, considering a random distribution. Probabilistic calculations based on the Poisson distribution, considering the Bohr-radius of isolated donor as ~ 2.4 nm, revealed that the domination of the formation of three triple-donor molecules.

Correspondingly, Fig. 1c portrays an over-all conduction band potential landscape in the slit region. Three distinct different deep potential wells due to three different donor-molecules are observed in one of the possible distribution, having the effective deepest potential of ~ 700 meV including an overall conduction band lowering of ~ 400 meV, arising out of interactions among all the donors.

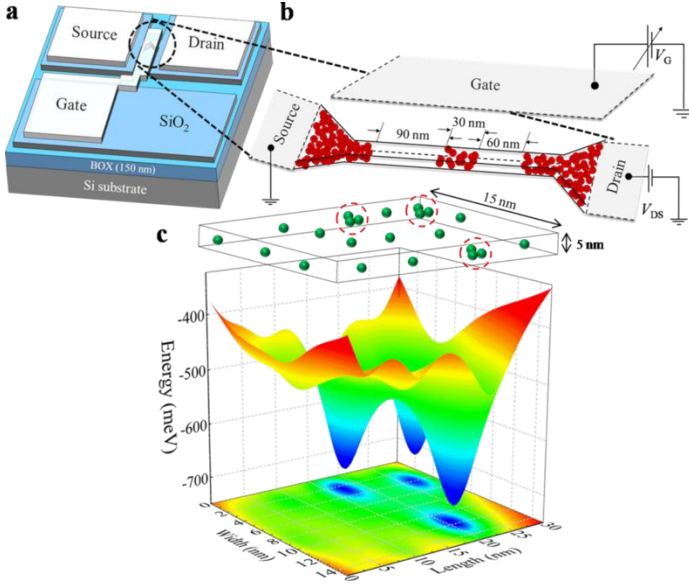


Fig. 1 Schematic Si nano-FET device configuration. **a**, Representation of the fabricated device as a silicon-on-insulator field-effect transistor (SOI-FET). **b**, Corresponding donor distribution within the channel region along with the top-gate design. **c**, An instance of donor distribution profile in the slit region of the nano-channel by employing a Poisson distribution approach. The corresponding probable potential landscape is simulated by approximating each isolated P-donor with a truncated Coulomb potential of the form $k\text{tanh}(\lambda r)/r$, within the spherical shell effective mass approximation. The values for $k = 1.67$ and $1/\lambda = 1.7$ nm are variationally set so that the isolated P-donor ground state energy converges to the bulk value of ~ 45 meV with an effective r_B of 2.4 nm.

Observation of quantum Coulomb blockade in a donor-molecule system

To characterize the device, we measure the corresponding stability diagram, depicting the evolution of the

differential-conductance dI_{DS}/dV_{DS} as a function of the bias voltage - gate voltage ($V_{DS} - V_G$) plane at $T = 5.5$ K (Fig. 2). The overview of stability diagram reveals well-organized and recurring pattern of six group of single-electron peaks (Group-1 to Group 6) each containing three distinct peaks. Low gate-bias single-electron peaks are accompanied by cross-biasing effects, where Coulomb diamonds become tilted and non-closed due to cross-talked between gate and source/drain.²¹ Such complicated and repetitive Coulomb oscillations cannot be correlated with transport via isolated donor atoms.^{22,23} In general, observation of large number of periodic Coulomb-oscillations can also be observed in geometrical QD induced by roughness, which is not in present scenario as the gap between the successive Coulomb-peaks are not following the QCB of a single QD and secondly, formation of such a small roughness-induced-QD in the present devices is highly negligible.²⁴ The observation of several groups of Coulomb-oscillations generally arises from series interactive QDs or parallel QDs. In case of series interaction, charge transport via interactive QDs can modify the number of Coulomb peaks along with the random variation in charging energies, which are not the present scenario.²⁵⁻²⁶ Other possible option is the transport through parallel non-interactive different QDs.²²⁻²³ Considering large periodicity of the Coulomb-oscillations, QDs must be very small in sizes. Formation of such small sizes geometrical QDs by a few numbers only is highly less likely in the present device fabrication process. Furthermore, considering the selectively doped channel region, formation of such QDs by interaction of multiple donors as like molecules is most feasible scenario as also supported by the probabilistic calculation as presented in Fig. 1c.²⁷⁻²⁹ In addition, the observation of several groups of Coulomb-peaks cannot be explained based on Mott-Hubbard impurity band,²⁸ where only two prominent bands (lower and upper Hubbard band) would be observed.

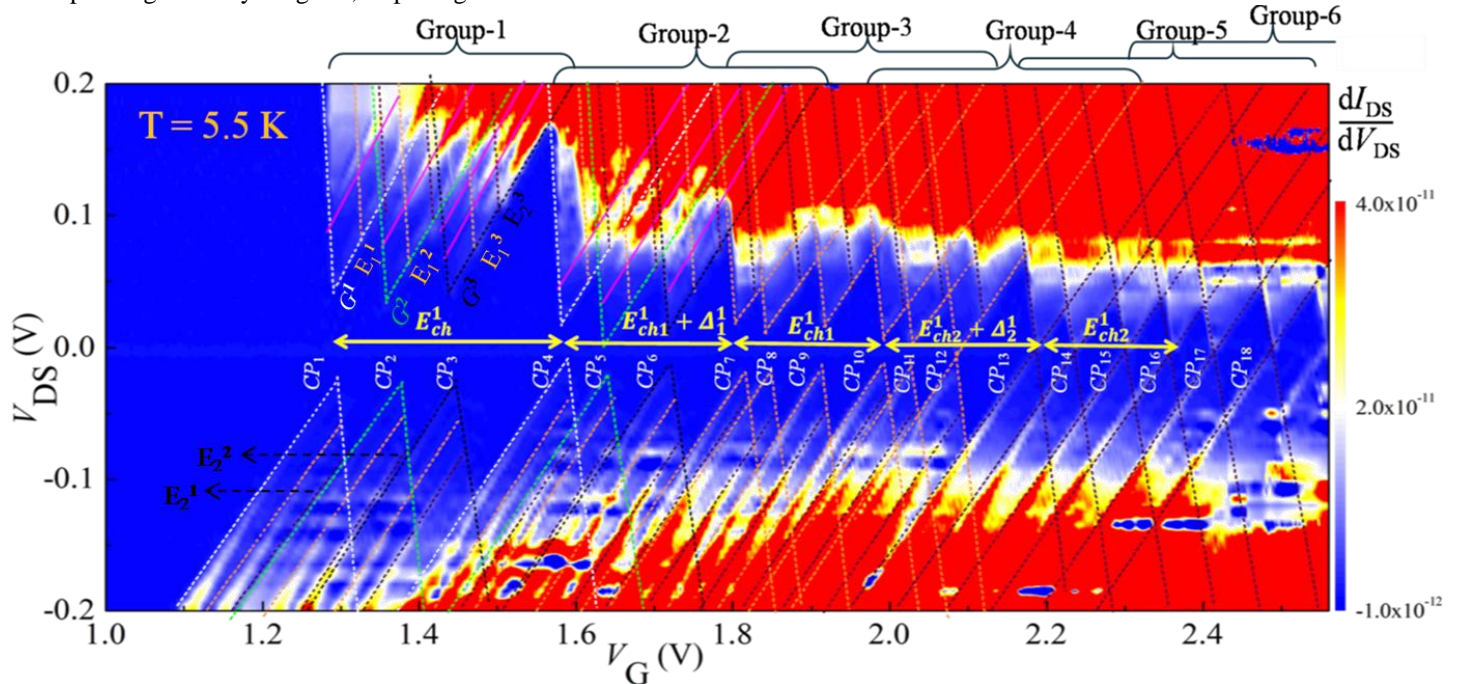


Fig. 2 Experimental electronic transport characteristics of the device. The conductance is plotted in the V_G - V_{DS} plane at $T = 5.5$ K. The observed successive Coulomb oscillations within Group-1 correspond to single-electron transport through the ground states of three different donor molecules, molecule-1, molecule-2, and molecule-3, respectively, where the successive ground-state features are highlighted by white (G^1), green (G^2) and black (G^3) dotted lines, respectively. The dark-yellow (E_1^1, E_1^2, E_1^3) and brown (E_2^1, E_2^2, E_2^3) dotted lines running parallel to the left-edges of the diamonds are the signatures of simultaneous electron transport through 1st and 2nd excited states of each molecule. Next successive groups of Coulomb oscillations, denoted by Group-1 to Group-6, correspond to electronic transport through the higher charge states and excited states of the donor-molecules, where 1st, 2nd and 3rd Coulomb peaks of each group correspond to electron transport through the isolated molecule-1, molecule-2 and molecule-3, respectively. The systematic evolutions of the color schemes of the electronic states represent the corresponding evolution of the different donor-molecule energy levels with the variation of applied bias-voltages. The transport lines, marked by pink, are the signatures of source LDOS which are observed only for the positive bias owing to the inherently asymmetric tunnel barriers at the source and drain side. The cross-biasing effect is also prominent on the initial few groups of Coulomb diamonds.

Thus the observed periodic and repetitive pattern of Coulomb-peaks plausibly originated due to active single-electronic transport from multiple individual multi-donor-induced QDs. Moreover, prominent signature of excited state lines, running parallel to the left-edges of the Coulomb-peaks, is observed.³⁰⁻³¹ Notably, every Coulomb peaks within group-1, 2 host two excited states each, which systematically decrease by one for every two successive Groups. The boundaries within each of the Coulomb-peaks that signify the onset of electronic-transport through ground, first and second excited states of the QDs are denoted by G, E_1, E_2 , respectively (Fig. 2). Correspondingly, the synonymous V_G - V_{DS} co-ordinates are tabulated in Table-1.

Further, the extracted Lever-arm factors ($\alpha = C_G/C_G + C_S + C_D$) for $CP_1 - CP_3$ are found to be approximately 0.95, 0.94 and 0.928, respectively. The calculated energy-differences between $G - E_1$, i.e. Δ_1 , and between $E_1 - E_2$, i.e. Δ_2 , are also different for $CP_1 - CP_3$ as observed from Fig. 2 and tabulated in Table-1. Thus, CP_1, CP_2, CP_3 are indeed from three different QDs, namely, QD_1, QD_2, QD_3 respectively. Consequently, we denote the $G, E_1, E_2, \Delta_1, \Delta_2$ of the three QDs by $G^i, E_1^i, E_2^i, \Delta_1^i, \Delta_2^i$, respectively, with i defining the QD index.

Correlating the identical characteristics, along-with striking similarities, in Δ_1^1 and Δ_2^1 values between CP_1 and CP_4 , they must be the first and second charge states, respectively, of the ground-state energy level for QD_1 . The corresponding charging-energy, extracted from the intersections of the extended slopes of CP_1 and CP_4 , is found to be ~ 280 meV (Figs. 2; Table1) and the corresponding ground state Bohr radius is $r_B \approx 0.43$ nm; calculated utilizing the relation $E_{ch} = e/C_\Sigma$. C_Σ is the self-capacitance of the dot given by $C_\Sigma = 4\pi\epsilon_{Si}r_B$ with ϵ_{Si} being the permittivity of the Si ≈ 11.9 .¹⁶ Moving along the V_G -axis, Δ_1^1 for CP_7 and CP_{10} exactly resemble Δ_2^1 of CP_1, CP_4 , affirming them to be 3rd and 4th charge state, respectively, of QD_1 . This is also consistent with the presence of a single excited state in CP_7 and CP_{10} , in contrast to the two excited states observed in CP_1 and CP_4 . The respective addition energies would thus precisely be $E_{ch1}^1 + \Delta_1^1$ and $E_{ch1}^1 + \Delta_2^1$ (Fig. 2 and Table 1), signifying clear signatures of QCB. The corresponding Bohr radius is calculated to be $r_B \approx 0.77$ nm. Further correlating the systematically decremental charging energy, CP_{13} and CP_{16} would be the 5th and 6th charge states, consistent with the absence of any excited state signatures within, of the QD_1 with respective addition energies of $E_{ch2}^1 + \Delta_1^1$ and $E_{ch2}^1 + \Delta_2^1$. Corresponding $r_B \approx 1.01$ nm.

Similarly, CP_2 and CP_5 arise due to single-electron transfer through the 1st and 2nd charge states of QD_2 with charging-energy E_{ch}^2 and $r_B \approx 0.452$ nm. CP_3 and CP_6 correspond to the 1st and 2nd charge states of QD_3 with charging-energy E_{ch}^3 and $r_B \approx 0.464$ nm. CP_8 and CP_{11} corresponds to the 3rd and 4th charge state configurations of QD_2 , with addition energies $E_{ch1}^2 + \Delta_1^2, E_{ch1}^2 + \Delta_2^2$, respectively and $r_B \approx 0.805$ nm. On-the-same-note, CP_9 and CP_{12} represent the 3rd and 4th charge state of QD_3 , with addition energies $E_{ch1}^3 + \Delta_1^3, E_{ch1}^3 + \Delta_2^3$, respectively and $r_B \approx 0.833$ nm. Consistent with the dynamics, CP_{14} and CP_{17} are the 5th and 6th charge states of the QD_2 with respective addition energies of $E_{ch2}^2 + \Delta_1^2$ and $E_{ch2}^2 + \Delta_2^2$, whereas, CP_{15} and CP_{18} are the 5th and 6th charge states of the QD_3 with addition energies of $E_{ch2}^3 + \Delta_1^3$ and $E_{ch2}^3 + \Delta_2^3$, respectively. The corresponding r_B for both QD_2 and QD_3 in these charge states are ≈ 1.05 nm.

The observed small r_B of the QDs, coupled with significant energy level separations and high charging-energies (Table-1), strongly indicate that they are plausibly originated from multi-donor interactions. Presence of three distinctly separated energy levels within each QD suggests that three closely spaced P-donors interacted to form each of the QDs. Additionally the absence of any modulations of the Coulomb peak edges while crossing each-other, demands the QDs are non-interacting.³

The observed systematic decrement of charging-energies for the successive higher energy levels of the QDs are reasonable as the electronic wave-functions become more spatially delocalized, leading to reduced effective Coulomb repulsion. This delocalization, coupled with the larger spatial extent of higher energy orbitals, increases the effective volume over which the electron charge is distributed.³² Thus, coupling of the QDs with the leads and correspondingly the capacitances increase³³⁻³⁴ leading to decreased charging energies followed by a similar trend in the observed α -values for successive Coulomb-peaks, which reaches approximately 0.67, 0.646 and 0.62, for CP_{16} - CP_{18} respectively. This could also be attributed to the effect of cross bias effect as presented in our previous work.²¹ So, the calculated charging-energies of the QD ground-states and the 1st-excited states may be overestimated.

Using these α -values, the estimated positions of the three non-interacting QDs, from the source reservoir, are ~ 111 nm, ~ 108 nm, ~ 118 nm, respectively²⁴ and the corresponding ionization energies are be ~ 840 meV, ~ 780 meV and ~ 700 meV considering the conduction band edge to be ~ 2560 mV.

Additional faint lines are observed within the first two Coulomb peak groups, running parallel to their right edges (marked in Fig. 2). These features are visible only for the positive bias condition, and can be most probably ascribed to random fluctuations in local density of states (LDOS) of the source reservoir.³⁵⁻³⁷ The absence of these lines in the negative bias can be attributed to the intentionally fabricated asymmetric tunnel barriers formation.³⁸

One-by-one electron filling in the molecular orbitals based on the concept of QCB

To decipher the detailed QCB transport mechanism, we describe the electron filling process within the observed potential landscape, as presented schematically in Figs. 3a-g with the experimentally measured energy scales. We analyze the sequential occupation of discrete electronic states of molecule-1, one of the three transport-active molecules. The electronic transport initiates when the lowest-lying and empty G^1 state aligns with the bias window through gate voltage adjustment (Fig. 3b). Consequently, the peak CP_1 arises (Fig. 3b) and is due to the 1st charge state of G^1 . Further increasing V_G , G^1 surpasses the source Fermi level and a single electron is trapped in the G^1 ; consequently, the energy of molecule-1 virtually enhances by E_{ch}^1 (marked by black dotted line in Fig. 3c) corresponding to the ground state, leading to the transport being blocked. Applying V_G equivalent to E_{ch}^1 , the singly-filled G^1 level, in the 2nd charge state configuration, realigns within the bias window (Fig. 3c) permitting another single-electron transport and CP_4 is observed; the Pauli Exclusion Principle prevents further electron transport via this ground state. Further electronic transport through the doubly-occupied molecule-1 can be facilitated by aligning the next empty E_1^1 level, Δ_1^1 away from G^1 with the bias window which would require corresponding charging-energy (E_{ch1}^1) added with Δ_1^1 to be provided and the Coulomb-peak CP_7 would be observed (Fig. 3d). To lift the next blockade, a further increment of the molecule-1 potential by E_{ch1}^1 is required and, electron will tunnel via the 2nd charge state of E_1^1 for the triply-occupied molecule-1 (Fig. 3e) to facilitate CP_{10} . Similarly, the next unoccupied energy level E_2^1 would actively participate in the transport with the 1st and 2nd charge state configurations upon successively applying gate voltages equivalent to energy $E_{ch2}^1 + \Delta_1^1$ and $E_{ch2}^1 + \Delta_2^1$ and we will observe CP_{13}, CP_{16} respectively. This is schematically presented in Figs. 3f-g. Identically, the other two molecules, molecule-2 and molecule-3, facilitate systematic electron transport based on the concept of QCB and the overall experimental transport characteristics of Fig. 2 is observed.

Table 1 Comprehensive description of the onset of single-electron transport through different energy levels of the three donor-molecules. The corresponding values in the V_G - V_{DS} plane are extracted from the experimental stability diagram of Fig 2. Based on these values, the corresponding charging-energies and energy separations between ground and different excited states of the isolated molecules are calculated, based on the concept and formalism of QCB.

Peak No.			1	4	7	10	13	16
Molecule 1	Approximate Peak Positions in mV for	$G^1(V_G, V_{DS})$	1290, 50	1580, 20	1800, 20	1988, 10	2188, 0	2362, 0
		$E_1^1(V_G, V_{DS})$	1328, 85	1618, 55	1830, 45	2022, 35	Not Observed	Not Observed
		$E_2^1(V_G, V_{DS})$	1356, 110	1646, 80	Not Observed	Not Observed	Not Observed	Not Observed
		$\Delta_1^1 = E_1^1 - G^1 = 35 \text{ meV}$	$E_{ch}^1 = 280 \text{ meV}$		$E_{ch1}^1 = 155 \text{ meV}$		$E_{ch2}^1 = 120 \text{ meV}$	
		$\Delta_2^1 = E_2^1 - E_1^1 = 25 \text{ meV}$		$E_{ch1}^1 + \Delta_1^1 = 190 \text{ meV}$		$E_{ch2}^1 + \Delta_2^1 = 145 \text{ meV}$		
Peak No.			2	5	8	11	14	17
Molecule 2	Approximate Peak Positions in mV for	$G^2(V_G, V_{DS})$	1358, 40	1636, 5	1842, 15	2026, 0	2236, 0	2414, 0
		$E_1^2(V_G, V_{DS})$	1386, 65	1664, 30	1884, 50	2070, 35	Not Observed	Not Observed
		$E_2^2(V_G, V_{DS})$	1422, 100	1704, 65	Not Observed	Not Observed	Not Observed	Not Observed
		$\Delta_1^2 = E_1^2 - G^2 = 25 \text{ meV}$	$E_{ch}^2 = 267 \text{ meV}$		$E_{ch1}^2 = 150 \text{ meV}$		$E_{ch2}^2 = 115 \text{ meV}$	
		$\Delta_2^2 = E_2^2 - E_1^2 = 35 \text{ meV}$		$E_{ch1}^2 + \Delta_1^2 = 175 \text{ meV}$		$E_{ch2}^2 + \Delta_2^2 = 150 \text{ meV}$		
Peak No.			3	6	9	12	15	18
Molecule 3	Approximate Peak Positions in mV for	$G^3(V_G, V_{DS})$	1438, 50	1720, 25	1916, 20	2084, 0	2302, 0	2488, 0
		$E_1^3(V_G, V_{DS})$	1466, 75	1750, 50	1954, 50	2124, 30	Not Observed	Not Observed
		$E_2^3(V_G, V_{DS})$	1500, 105	1784, 80	Not Observed	Not Observed	Not Observed	Not Observed
		$\Delta_1^3 = E_1^3 - G^3 = 25 \text{ meV}$	$E_{ch}^3 = 260 \text{ meV}$		$E_{ch1}^3 = 145 \text{ meV}$		$E_{ch2}^3 = 115 \text{ meV}$	
		$\Delta_2^3 = E_2^3 - E_1^3 = 30 \text{ meV}$		$E_{ch1}^3 + \Delta_1^3 = 170 \text{ meV}$		$E_{ch2}^3 + \Delta_2^3 = 145 \text{ meV}$		

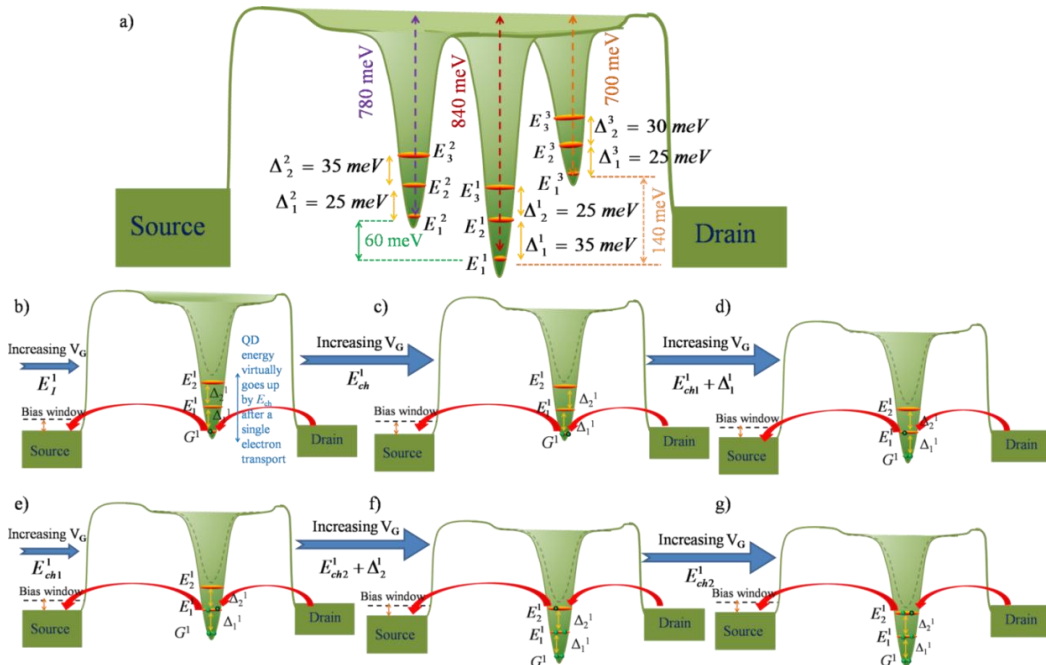


Fig. 3 Schematic representation of QCB transport. a, Deduced energy-level scheme of the three isolated-donor molecules. **b-g,** One-by-one electron transport and filling in the different charge states of successive energy levels within one of the three isolated transport-active donor-molecules, namely molecule-1, with the evolution of gate bias voltage.

First-principles insights into molecular-orbital structures

To obtain a qualitative understanding of the observed energy spectra and the nature of the energy levels participating in the transport, we perform first-principles simulations of silicon nanostructures containing three closely spaced P-donors, as shown in Fig. 4a. For that, we conducted Density Functional Theory (DFT) calculations using Quantum-ATK software.³⁹ First, we constructed a silicon nanowire with a diameter of approximately 1.6 nm and a length of 5.4 nm. To minimize the influence of surrounding atoms, we introduced a 1 nm vacuum region around the nanowire. Three P-donors were substituted into the Si matrix, as illustrated in Fig. 4a, representing a plausible experimental scenario for the 3-donor molecules. The nanowire dimensions are smaller than those in typical experimental devices due to computational resource limitations.

Figure 4b demonstrates the total-density-of-states (TDOS) spectra of the 3-donors, individually and cumulatively, where the lowest three energy levels, marked by G , E_1 , E_2 respectively, qualitatively correspond to the experimentally observed lowest-lying energy levels of either of the three molecules that are actively participating in the transport.

This splitting is consistent with the expectation that the number of split levels within the GS manifold correlates with the number of strongly coupled donors. The separation between these ground-state levels qualitatively matches experimental observations and have almost the same ratio of $\Delta_1^2 : \Delta_2^2 : E_l^2 \equiv 1 : 1.4 : 33$, reasonably close to the spectra for molecule-1 and molecule-2. Therefore, this arrangement can be considered as the most likely configuration of the three individual donors that constitutes the donor-molecules. The projected-density-of-states (PDOS) at the location of each P donor are also shown in Fig. 4c, where different colors indicate contributions of s , p , d orbitals of the left, middle and right donors at their respective locations. Fig. 4d signifies the relative weight of donor states against the states of the whole system⁴⁰⁻⁴¹ and corresponding ionisation energy of the donor-molecule is found to be ≈ 1.2 eV. Furthermore, the orbital-decomposed PDOS of the donors indicates that the split ground-state levels are primarily-derived from the s orbitals of the donors whereas, the third level of ground-state-manifold and further excited-states of the simulated are resulting from hybridization of the s , p , and d orbitals, which is qualitatively different from simple multi-donor clusters, where the ground-state manifolds originate mostly due to interactions from s -orbitals only.¹⁷

Simulation for the observed QCB effects

To investigate the validity of the actual scenario within the theoretical framework, we construct an equivalent-capacitor circuit model incorporating three parallel molecules involved in electron tunneling and reproduce the experimental stability diagram at $T = 5.5$ K using modified rate equation approach⁴² equipped for QCB (Figs. 5a-b). Within the simulated stability diagram (Fig. 5b), we observe traces of all the discrete energy levels, that actively participated in the experimental electron transport through the device, along with the LDOS features. Moreover, the systematic modulation of the charging-energies corresponding to the different energy levels of the three distinct molecules, are also reflected within the simulated results. The quantitative and qualitative similarities between the experimental and simulated stability diagrams (Fig. 2, Fig. 5b) and different energy scales like ionization and charging-energies confirm the validity of QCB single-electron transport through three-isolated donor-molecules. The slight qualitative mismatch in the initial

few Coulomb peak shapes is most-likely originated due to the exclusion of cross-biasing effects²¹ within the simulation. This does not however impact the overall conclusions.

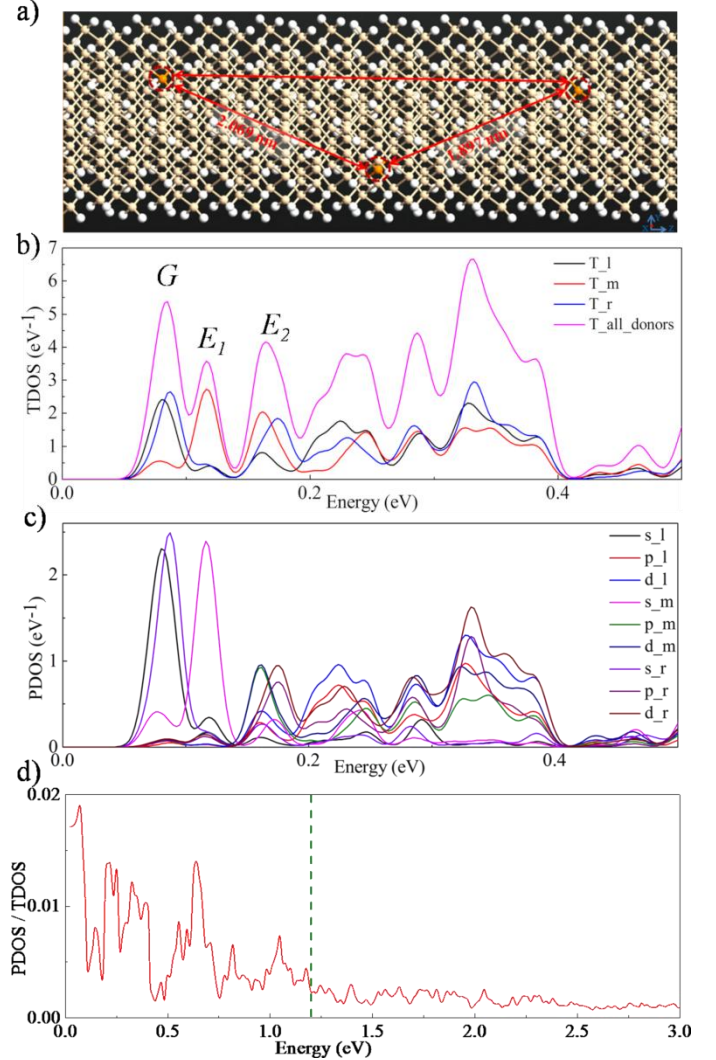


Fig. 4 First-principles analysis of nanostructures containing 3-P donors. The DFT calculations were carried out using the Linear Combination of Atomic Orbitals (LCAO) method, with the Generalized Gradient Approximation (GGA) approach to handle exchange-correlation interactions, employing the PBE Double Zeta Polarized functional. The k-point density was set to $(1 \times 1 \times 4)$, with a grid mesh cutoff of 45 Hartree. Geometry optimization was performed using the LBFGS optimizer, with a self-consistent field iteration tolerance of 0.0001 Hartree. During optimization, lattice parameters and atomic positions were adjusted until atomic forces were reduced to below 0.05 eV/Å. **a**, Atomistic view of the simulated nanostructure, containing P-donors (distance between P_1 - P_2 and P_2 - P_3 is ~ 2.06 nm and ~ 1.89 nm, respectively). **b**, The corresponding TDOS spectrum contributions from each donor of the molecule and the overall TDOS spectrum. l , m , r defines the left, middle, right donor atoms respectively. Δ_1 , Δ_2 are found to be ≈ 34 meV and ≈ 48 meV, respectively. **c**, Respective individual orbital contributions from each donor, constituting the TDOS. s , p , d suggests the atomic orbitals. **d**) PDOS / TDOS spectra of the P-donor-molecule. The ionisation energy is estimated by taking the ratio of PDOS/TDOS, which signifies the relative weight of donor states against the states of the whole system. In the lower energy range, the contribution from the donor is dominated but, the contribution is trivial at higher energy range (above the green dashed line) due to the inclusion of more number of silicon atoms. The ionisation energy is calculated from the point where this ratio saturates close to 0 and found to be around 1.2 eV.

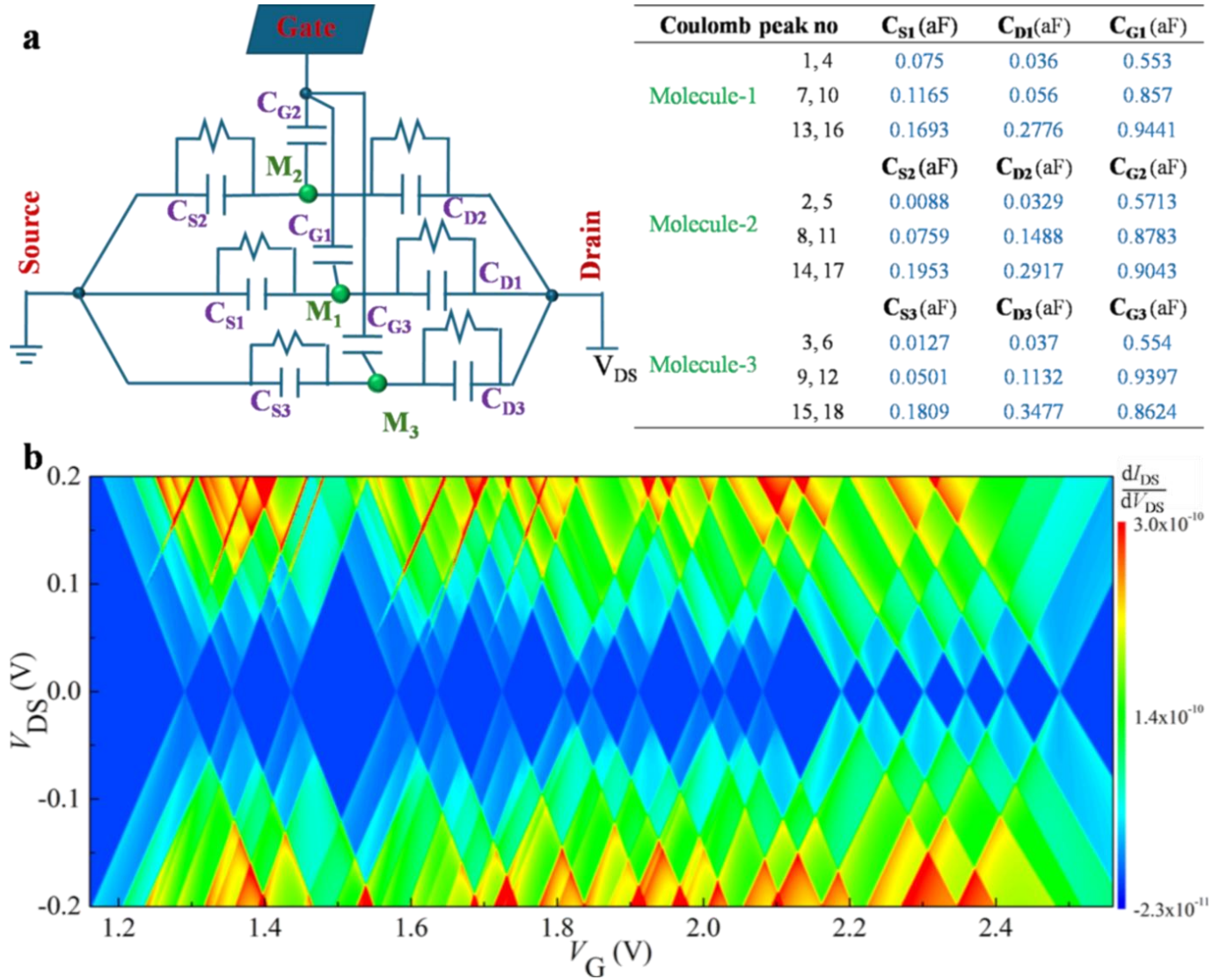


Fig. 5 Simulation of the overall transport characteristics within modified rate equation approach. a, Schematic equivalent capacitor circuit diagram of the studied device. Blue dots represent nodes in the circuit connection whereas the green spheres represent the three isolated donor molecules that actively participate in the single-electron transport. **b,** The corresponding simulated stability diagram at $T = 5.5$ K for the same configuration.

Conclusions

In conclusion, we experimentally demonstrate an initial observation of QCB in Si nano-FET, where systematic one-by-one molecular-like filling of six electrons is achieved within the GS manifolds of each of the three isolated, three P-donor molecular systems. Furthermore, we have discussed the evolution and systematic decrement of charging-energies in correlation with the increasing spatial extent of successive higher molecular energy levels. The origin of such molecular levels due to orbital hybridization of the constituent individual donors is also described by first-principle-simulations using DFT. The observed QCB characteristics are further corroborated through modified-rate-equation simulation based on QCB. Moreover, the observed high charging-energies of few hundred meV and ionization-energies around 800 meV, along with approximate separations of 30 meV between successive energy levels of the donor-molecules, reflect the feasibility of such devices for the implementation of high-temperature single-electron tunneling and charge-qubit operation, at least up to mid-range temperatures.

Methods

Device fabrication

The device is fabricated on the silicon-on-insulator (SOI) platform comprised of a buried oxide (BOX) layer of 150 nm thickness and an initial silicon device layer of 55 nm thickness. Upon patterning the constricted nano-wire channel

with length and width of approximately 180 nm and 15 nm, respectively, by an electron-beam lithography technique, a 30 nm \times 15 nm opening was created, 90 nm away from the source and drain reservoir, which was further doped with P-donor concentration of $N_D \approx 10^{19} \text{ cm}^{-3}$. Through the standard and sacrificial oxidation processes during the fabrication steps, the device layer is reduced to approximately 5 nm. Such heavily-doped nano-slit contains approximately 22 donors, with the average inter-donor spacing of ~ 1.5 nm, suggesting strong interaction among the donors to facilitate multi-donor cluster formation. All fabrication processes are conducted in a clean-room environment and follow CMOS-compatible methodologies. After the channel patterning, the top oxide layer of thickness approximately 10 nm is grown by thermal dry oxidation at 800°C for 15 minutes, as a final gate oxide. Aluminum (Al) was used for the gate, source, and drain contacts.

Electrical measurements

Electrical measurements are conducted utilizing an Agilent 4156C precision semiconductor parameter analyzer coupled to a variable-temperature probe station. All current-voltage (I - V) measurements are performed in high vacuum. During all the measurements, the source and substrate remain grounded, while bias is applied to the drain electrode as V_{DS} . Top-gate is used to control the charge-states of the donors in the channel region, by the gate voltage V_G .

Data availability

The data that support the findings of this study are available within the article.

References

1. H. Sellier, G. P. Lansbergen, J. Caro, S. Rogge, N. Collaert, I. Ferain, M. Jurczak, and S. Biesemans, *Phys. Rev. Lett.* **97**, 206805 (2006).
2. M. Tabe, D. Moraru, M. Ligowski, M. Anwar, R. Jablonski, Y. Ono, and T. Mizuno, *Phys. Rev. Lett.* **105**, 016803 (2010).
3. M. Pierre, R. Wacquez, X. Jehl, M. Sanquer, M. Vinet, and O. Cueto, *Nat. Nanotechnol.* **5**, 133 (2010).
4. J. Verduijn, G. C. Tettamanzi, and S. Rogge, *Nano Lett.* **13**, 1476 (2013).
5. A. Samanta, D. Moraru, T. Mizuno, M. Tabe, *Sci. Rep.* **5** (1), 17377 (2015).
6. S. Chakraborty, A. Samanta, *Adv. Quantum Technol.* **7**, 2300349 (2024).
7. F. A. Zwaneburg, A. S. Dzurak, A. Morello, M. Y. Simmons, L. C. L. Hollenberg, G. Klimeck, S. Rogge, S. N. Coppersmith, and M. A. Eriksson, *Rev. Mod. Phys.* **85**, 961 (2013).
8. J. Gorman, D. G. Hasko, and D. A. Williams, *Phys. Rev. Lett.* **95**, 090502 (2005).
9. G. P. Lansbergen, R. Rahman, C. J. Wellard, I. Woo, J. Carro, N. Collaert, S. Biesemans, G. Klimeck, L. C. L. Hollenberg, and S. Rogge, *Nat. Phys.* **4**, 656, (2008).
10. V. V. Shorokhov, D. E. Presnov, S. V. Amitonov, Yu. A. Pashkin, and V. A. Krupenin, *Nanoscale* **9**, 613 (2017).
11. M. Fuechsle, J. A. Miwa, S. Mahapatra, H. Ryu, S. Lee, O. Warschkow, L. C. L. Hollenberg, G. Klimeck, and M. Y. Simmons, *Nat. Nanotechnol.* **7**, 242 (2012).
12. M. Diarra, Y.-M. Niquist, C. Delerue, and G. Allan, *Phys. Rev. B* **75**, 045301 (2007).
13. M. T. Bjork, H. Schmid, J. Knoch, H. Riel, and W. Riess, *Nat. Nanotechnol.* **4**, 103 (2009).
14. M. Pierre, R. Wacquez, X. Jehl, M. Sanquer, M. Vinet, and O. Cueto, *Nat. Nanotechnol.* **5**, 133, (2010).
15. D. Moraru, A. Samanta, K. Tyszka, L. T. Anh, M. Muruganathan, T. Mizuno, R. Jablonski, H. Mizuta, and M. Tabe, *Nanoscale Res. Lett.* **10**, 372 (2015).
16. A. Samanta, M. Muruganathan, M. Hori, Y. Ono, H. Mizuta, M. Tabe, and D. Moraru, *Appl. Phys. Lett.* **110**, 093107 (2017).
17. D. Moraru, A. Samanta, L. T. Anh, T. Mizuno, H. Mizuta, and M. Tabe, *Sci. Rep.* **4**, 6219 (2014).
18. B. Weber, Y. H. M. Tan, S. Mahapatra, T. F. Watson, H. Ryu, R. Rahman, L. C. L. Hollenberg, G. Klimeck, and M. Y. Simmons, *Nat. Nanotechnol.* **9**, 430 (2014).
19. L. P. Kouwenhoven, T. H. Oosterkamp, M. W. S. Danoesastro, M. Eto, D. G. Austing, T. Honda, and S. Tarucha, *Science* **278**, 1788 (1997).
20. G. A. Thomas, M. Capizzi, F. De Rosa, R. N. Bhatt, and T. M. Rice, *Phys. Rev. B* **23**, 5472 (1981).
21. A. Afiff, A. Samanta, A. Udhiarto, H. Sudibyo, M. Hori, Y. Ono, M. Tabe, and D. Moraru, *Appl. Phys. Express* **12**, 085004 (2019).
22. D. Moraru, A. Udhiarto, M. Anwar, R. Nowak, E. Hamid, T. Mizuno, and M. Tabe, *Nanoscale Res. Lett.* **6**, 479 (2011).
23. E. Prati, R. Latempa, and M. Fanciulli, *Phys. Rev. B* **80**, 165331 (2009).
24. S. Chakraborty, P. Yadav, D. Moraru, and A. Samanta, *Adv. Quantum Technol.* **7** (7), 2400011 (2024).
25. C. Hong, G. Yoo, J. Park, M. K. Cho, Y. Chung, H. S. Sim, D. Kim, H. Choi, V. Umanski, and D. Mahalu, *Phys. Rev. B* **97**, 241115 (R) (2018).
26. S. Imami, *Jpn. J. Appl. Phys.* **50**, 034302 (2011).
27. M. Liuhong, H. Weihua, H. Wang, H. Wenting, L. Qifeng, X. Yang, and F. Yang, *J. Appl. Phys.* **117**, 034505 (2015).
28. A. Afiff, A. Samanta, A. Udhiarto, H. Sudibyo, M. Hori, Y. Ono, M. Tabe, and D. Moraru, *Appl. Phys. Express* **12**, 085004 (2019).
29. M. F. G. Zaiba, A. Saravia, M. J. Calderon, D. Heiss, B. Koiler, and A. J. Ferguson, *Nano Lett.* **14**, 10, 5672 (2014).
30. I. A. Verzhbitskiy, A. Mishra, S. Mitra, Z. Zhang, S. Das, C. S. Lau, R. Lee, D. Huang, G. Eda, Y. S. Ang, and K. E. J. Goh, *ACS Nano* **19**, 11, 10878 (2025).
31. Huebl, H. *et al.* Phosphorus donors in highly strained silicon. *Phys. Rev. Lett.* **97**, 166402 (2006).
32. T. H. Ning and C. T. Sah, *Phys. Rev. B* **4**, 3468 (1971).
33. N. Y. Morgan, D. A. Magder, M. A. Kastner, Y. Takahashi, H. Tamura, and K. Murase, *J. Appl. Phys.* **89**, 410 (2001).
34. E. Foxman *et al.*, *Phys. Rev. B* **47**, 10020 (1993).
35. J. Zhengyang, X. Caigan, J. Chen, Y. Ouyang, F. Wang, M. Zhang, and F. Song, *Nanoscale* **16**, 6309, (2024).
36. M. Möttönen, K. Y. Tan, K. W. Chan, F. A. Zwanenburg, W. H. Lim, C. C. Escott, J. M. Pirkkalainen, A. Morello, C. Yang, J. A. van Donkelaar, A. D. C. Alves, D. N. Jamieson, L. C. L. Hollenberg, and A. S. Dzurak, *Phys. Rev. B* **81**, 161304(R) (2010).
37. H. Buch, M. Fuechsle, W. Baker, M. G. House, and M. Y. Simmons, *Phys. Rev. B* **92**, 235309 (2015).
38. T. Schmidt, R. J. Haug, V. I. Fal'ko, K. V. Klitzing, A. Förster, and H. Lüth, *Phys. Rev. Lett.* **78**, 1540 (1997).
39. S. Smidstrup, T. Markussen, P. Vancraeyveld, J. Wellendorff, J. Schneider, T. Gunst, B. Verstichel, D. Stradi, P. A. Khomyakov, U. G. Vej-Hansen, M. E. Lee, S. T. Chill, F. Rasmussen, G. Penazzi, F. Corsetti, A. Ojanperä, K. Jensen, M. L. N. Palsgaard, U. Martinez, A. Blom, M. Brandbyge, and K. Stokbro, *J. Phys. Condens. Mat* **32**, 1 (2020).
40. L. Te. Anh, D. Moraru, M. Manoharan, M. Tabe, and H. Mizuta, *J. Appl. Phys.* **116**, 063705 (2014).
41. P. Yadav, H. Arora, and A. Samanta, *Appl. Phys. Lett.* **122**, 083502 (2023).
42. P. Yadav, S. Chakraborty, D. Moraru, and A. Samanta, *Nanomater.* **12**, 4437 (2022).